Growth of metallic delafossite PdCoO$_2$ by molecular beam epitaxy

Matthew Brahlek,[1,*] Gaurab Rimal,[2] Jong Mok Ok,[1] Debangshu Mukherjee,[3] Alessandro R. Mazza,[1] Qiyang Lu,[1]
Ho Nyung Lee,[1] T. Zac Ward,[1] Raymond R. Unocic,[3] Gyula Eres,[1] and Seongshik Oh[2,†]

[1]*Materials Science and Technology Division, Oak Ridge National Laboratory, Oak Ridge, Tennessee 37831, USA*
[2]*Department of Physics and Astronomy, Rutgers, The State University of New Jersey, Piscataway, New Jersey 08854, USA*
[3]*Center for Nanophase Materials Sciences, Oak Ridge National Laboratory, Oak Ridge, Tennessee 37831, USA*

The Pd- and Pt-based ABO$_2$ delafossites are a unique class of layered, triangular oxides with two-dimensional electronic structure and a large conductivity that rivals the noble metals. Here, we report successful growth of the metallic delafossite PdCoO$_2$ by molecular beam epitaxy (MBE). The key challenge is controlling the oxidation of Pd in the MBE environment where phase segregation is driven by the reduction of PdCoO$_2$ to cobalt oxide and metallic palladium. This is overcome by combining low-temperature (300 °C) atomic layer-by-layer MBE growth in the presence of reactive atomic oxygen with a postgrowth high-temperature anneal. Thickness dependence (5–265 nm) reveals that in the thin regime (<75 nm), the resistivity scales inversely with thickness, likely dominated by surface scattering; for thicker films, the resistivity approaches the values reported for the best bulk crystals at room temperature, but the low-temperature resistivity is limited by structural twins. This work shows that the combination of MBE growth and a postgrowth anneal provides a route to creating high-quality films in this interesting family of layered, triangular oxides.

Confining three-dimensional (3D) electron systems to 2D or 1D is a well-established route to observe and control quantum phenomena. Such effects arise naturally in a wide range of materials systems where the dimensionality of the crystal lattice naturally gives rise to 2D or 1D electronic structure. An interesting example are the unique ABO$_2$ delafossite oxides. The electronic structure is highly 2D due to natural A-BO$_2$ layering, where the BO$_2$ layer is composed of edge-sharing BO$_6$ oxygen octahedra, and the A layers are ionically bonded vertically above and below the oxygen atoms [1]. The delafossites come in two electronic motifs [2]. The first are the insulators, which have been extensively studied as p-type transparent conductors when degenerately doped [3,4]. Here, the A-site cations are, for example, Ag or Cu, and the B-site cations are typically either a transition metal or a trivalent p-block metal, for example Al or Ga. The second class are the metallic compounds where A = Pd or Pt, and the B-site cations are transition metals Co, Cr, or Rh (AgNiO$_2$, a delafossite polytype, is also metallic [5,6]). In the metallic phase, the A-site cations are in a 1^+ valence state, which is unusual for elements such as Pd and Pt. The low-temperature conductivity reported in these metallic compounds is the highest reported for any oxide material, as high as 1.3×10^8 S/cm and mean free paths in excess of 20 μm [7]. Further, the triangularly connected, highly localized states on the BO$_6$ octahedra offer an interesting platform for exploring the effects of frustrated magnetism coupled with the itinerant electrons in the A-layer

[8]. Together, these unique characteristics have combined to give rise to numerous exotic phenomena [6], including large interfacial Rashba-like spin splitting at the surface [9] as well as quantifying electron viscosity [9]. Yet, there is no report on the growth of these materials by molecular beam epitaxy (MBE), and only one report on growth by pulsed laser deposition (PLD) in the ultrathin limit [10]. Metallic delafossite films can be utilized for various electronic applications ranging from low-resistivity bottom electrodes for 2D materials to correlated transparent conductors [10,11]. The creation of well-controlled delafossite films will also enable answering many fundamental questions that cannot be readily addressed with bulk crystals, such as the effects of strain on electronic and magnetic properties, and dimensional confinement from 3D to 2D with reduced film thickness.

Here, we report on the growth of the prototypical metallic delafossite PdCoO$_2$ by MBE on c-plane Al$_2$O$_3$ substrates (see Ref. [12] for experimental details). It was found that using atomic oxygen plasma at pressures up to 4×10^{-6} Torr enabled PdCoO$_2$ to be grown only up to a temperature of about 300 °C. Beyond this temperature, PdCoO$_2$ spontaneously decomposed by losing oxygen and forming Pd metal and CoO, as confirmed by surface-sensitive reflection high-energy electron diffraction (RHEED), x-ray photoemission spectroscopy (XPS), and bulk sensitive x-ray diffraction (XRD). As such, confining the growth to low temperature resulted in poor crystalline quality, thus necessitating a postgrowth high-temperature anneal in an oxygen atmosphere. After annealing to $T_{ann} = 700$ °C in air and 800 °C in oxygen (as detailed in Ref. [12], films were annealed at T_{ann}, which, unless otherwise stated, refers to the air-annealing temperature), the crystalline quality improved substantially, the resistivity decreased, and the surfaces became atomically

---

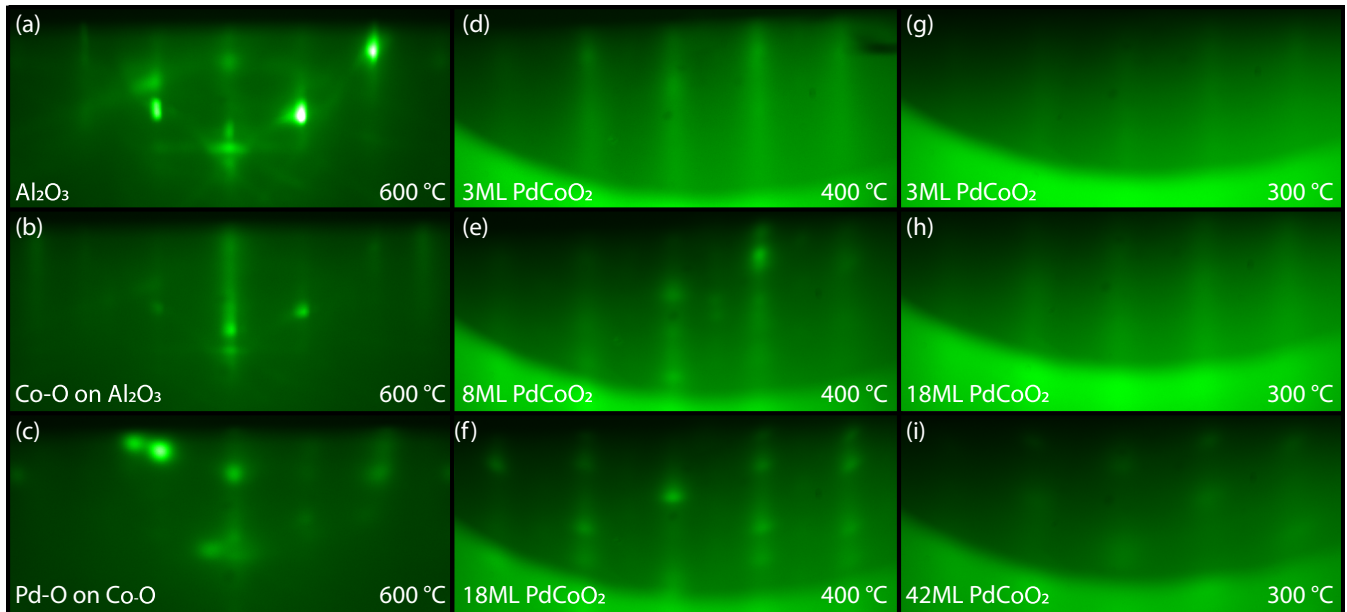*Author to whom all correspondence should be addressed: brahlekm@ornl.gov

†ohsean@physics.rutgers.edu

FIG. 1. Reflection high-energy electron diffraction (RHEED) images for the growth of PdCoO$_2$ on Al$_2$O$_3$ at various conditions. Images in (a), (b) are taken along the Al$_2$O$_3$ $\langle 100 \rangle$ and (d)–(i) are along the PdCoO$_2$ $\langle 100 \rangle$ azimuthal direction; temperature, material, and thickness are indicated in the figure. (a) Al$_2$O$_3$ substrate; (b), (c) Co-O monolayer (ML), then a Pd-O ML grown at 600 °C; (d)–(f) 3 ML (d), 8 ML (e), and 18 ML (f) PdCoO$_2$ grown at 400 °C; (g)–(i) 3 ML (g), 18 ML (h), and 42 ML (i) PdCoO$_2$ grown at 300 °C.

flat. Above this temperature, however, the films were found to phase-segregate, likely driven by sublimation of volatile PdO. The balance dictated by the behavior of oxidation of Pd places a narrow window where high-quality single-phase PdCoO$_2$ can be grown.

To find the optimal growth condition, various temperatures were used, and Fig. 1 shows examples of growth monitoring by RHEED at three different growth temperatures (300, 400, and 600 °C). The first attempts to grow PdCoO$_2$ were at a substrate temperature of 600 °C, which was motivated by two aspects: (i) For ternary oxides, typical growth temperatures around or above 600 °C are necessary to drive surface kinetics to enable crystallization; and (ii) the reaction of Pd with oxygen to form volatile PdO [13] on the growing surface can enable adsorption-controlled growth, for example in PbTiO$_3$ [14,15] and ruthenate perovskites [16] (see also Refs. [17,18] and references therein for more examples); the possible formation of volatile PdO is highlighted by PLD growth of PdCoO$_2$ where synthesis of Pd-deficient films necessitated alternating depositions from a PdCoO$_2$ target and a Pd-O target [10]. The real-time results from RHEED for deposition at 600 °C are shown in Figs. 1(a)–1(c), which provides structural and morphological information. Starting with Al$_2$O$_3$ along the $\langle 100 \rangle$ crystal direction in Fig. 1(a), RHEED shows bright well-defined spots and Kikuchi lines, indicating flat morphology and high structural quality. Under plasma oxygen at a pressure of 4×10^{-6} Torr at 450 W, a monolayer (ML) of Co was initially deposited, followed by a ML of Pd, shown in Figs. 1(b) and 1(c), respectively. RHEED measurements showed that immediately the crystal quality degraded (loss of peak intensity), and 2D morphology became 3D (streaks gave way to spots), and the targeted phase was lost (additional peaks appeared off the main peaks). This was most apparent

during the Pd deposition, which indicated that metallic Pd clusters form on the surface rather than the oxide.

The formation of metallic Pd clusters suggests the growth temperature was too high, which motivated the following strategy. The rule of thumb for achieving a conformal epitaxial metal film requires the growth temperature to be around 3/8 of the melting point of the metal [19]. For Pd, this temperature is 400 °C, which would enable the formation of a conformal film of Pd, and, when deposited in an oxygen environment, likely enables the formation of PdCoO$_2$. As such, it was found that a lower temperature of 400 °C combined with layer-by-layer deposition (Co-Pd-Co, …,Pd-Co), which followed the natural PdCoO$_2$ layering, was successful: on the other hand, codeposition failed to form the delafossite phase. To show the successful growth, RHEED images for the growth at 400 °C are shown in Figs. 1(d)–1(f). In panel (d), at 3 ML the resulting film (i) is single phase (no extra spots off the main peaks), (ii) has a 2D morphology (streaky pattern), and (iii) is structurally consistent with PdCoO$_2$ (this point will be confirmed later). As the thickness was increased, however, additional crystal phases appeared, as can be seen in Figs. 1(e) and 1(f) for 8 and 18 ML; this is seen as the appearance of distinct half-order-like additional peaks, which resemble RHEED images previously reported for the growth of Co$_3$O$_4$ on Al$_2$O$_3$ [20] (see also Fig. S1 for corresponding XRD scan). This suggests that 400 °C is on the boundary of stability. It is interesting, however, that the film is initially stable in the thin limit but gradually becomes unstable as the thickness increases, suggesting that proximity to the substrate, thickness, or both affect the thermodynamic stability. By lowering the temperature to 300 °C, it was found with RHEED that single-phase PdCoO$_2$ can be grown, as shown in Fig. 1(g) at 3 ML. As the thickness was increased, however, the morphology
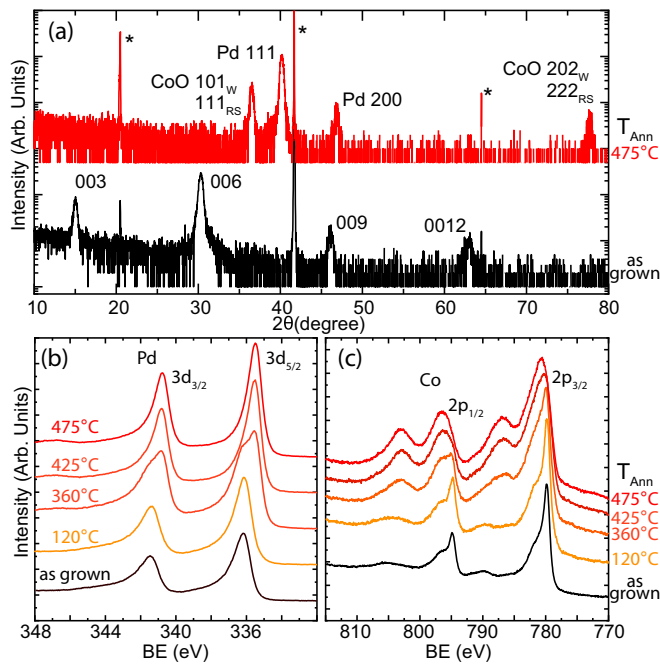
FIG. 2. Effect of vacuum annealing on the properties of PdCoO$_2$ films. (a) X-ray diffraction 2θ-θ scans for 25-nm-thick PdCoO$_2$ as grown at 300 °C (lower black curve labeled as-grown) and annealed in vacuum to 475 °C (upper red curve). The 003n labels mark the delafossite peaks, the asterisk (*) marks peaks belonging to Al$_2$O$_3$, and the subscripts on CoO indicate wurtzite (W) and rocksalt (RS). Curves are vertically offset for clarity. (b),(c) X-ray photoemission spectroscopy about Pd 3d (b) and Co 2d (c) for the as-grown film and while annealing in vacuum. Curves are vertically offset for clarity.

changed from 2D to 3D, but the phase remained that of PdCoO$_2$ (since no additional peaks appear), as can be seen by comparing Figs. 1(g) and 1(i) for thicknesses of 3 ML (g), 18 ML (h), and even up to 42 ML (i).

Figure 2(a) shows XRD 2θ-θ scans for PdCoO$_2$ films grown at 300 °C (labeled *as-grown*), as well as a sample that was annealed to 475 °C in vacuum. Other than the substrate peaks (marked by *), the lower black curve shows the 003n set of peaks, where n is an integer. This set of peaks is characteristic of the 3 ML periodicity of the unit cell of PdCoO$_2$ along the c-axis [1]. Furthermore, the lower, black-colored curves in Figs. 2(b) and 2(c) show XPS results for the as-grown film (see Ref. [12] for experimental details), where Figs. 2(b) and 2(c) show the results for Pd 3d and Co 2p states, respectively. The overall shape and binding energy agree with the results reported for bulk PdCoO$_2$ [21] with Pd^{1+} and Co^{3+}. Both the XRD and XPS data agree with the interpretation of the RHEED data and confirm that the as-grown films at 300 °C are single-phase PdCoO$_2$. These observations, however, indicate that the oxidation capabilities inherent to the MBE growth process (mainly pressure) limit the growth temperature and thus the structural quality of the PdCoO$_2$. Hence, a secondary postgrowth anneal is likely to improve the quality.

To see this, we systematically explored annealing conditions in vacuum and *ex situ* in air and oxygen: we first discuss the results for vacuum annealing and later return to *ex situ*

anneal. Shown in Figs. 2(b) and 2(c) are the temperature dependence of XPS spectra that were annealed in vacuum at 120, 360, 425, and 475 °C. With increasing annealing temperature, the peak positions of Pd 3$d_{3/2}$ and 3$d_{5/2}$ shifted between 360 and 425 °C to lower binding energies. Similarly, Co 2$p_{1/2}$ and 2$p_{3/2}$ peaks shifted toward higher binding energies. This is consistent with the reduction of Pd^{1+} to metallic Pd^{0+}, and the Co^{3+} reducing to Co^{2+} [21]. This is confirmed by XRD that was performed after the XPS anneal to 475 °C; see the upper red curve shown in Fig. 2(a). The PdCoO$_2$ peaks were gone, and additional peaks appeared at 36.5°, 40.2°, 46.8°, and 77.7° in 2θ: the peaks at 36.5° and 77.7° are CoO, either the 101 and 202 peaks of wurtzite or the 111 or 222 peaks of rocksalt [22,23], and the peaks at 40.2° and 46.8° agreed, respectively, with the 111 and 200 Pd peaks. This confirms that more oxidizing conditions are needed to improve the properties of PdCoO$_2$.

We now show the results for annealing PdCoO$_2$ films in air by starting with structural data, and below we discuss the effects on transport data. The evolution of XRD 2θ-θ curves for as-grown PdCoO$_2$ and air-annealed to 700 and 800 °C is shown in Fig. 3(a). In comparing the as-grown and 700 °C curves, it can be seen that both are free from any secondary phases (for annealed films, it is noted that a peak emerges in some thick films at 61°, which may be related to the formation of PdO). In going from 700 to 800 °C, an additional peak appears at around 39° in 2θ. This is most likely the 222 peak of Co$_3$O$_4$ [24]. The Co$_3$O$_4$ phase segregation is likely driven by the formation and evaporation of palladium oxide. The detailed structural evolution is shown in Fig. 3(b), where the intensity of the PdCoO$_2$ 006 and 0012 peaks and the 222 peak of Co$_3$O$_4$, normalized to the substrate 006 peak, is plotted versus annealing temperature. The intensity of the delafossite peaks is nominally constant until about 600 °C, and sharply increases in going from 600 to 800 °C by nearly an order of magnitude, indicating a large improvement to the structure of the film. However, by 800 °C the rise of the intensity of the Co$_3$O$_4$ peak shows that, although the structural quality of the PdCoO$_2$ continues to improve, it becomes unstable. When the film was annealed in pure oxygen instead, the film remained in single phase up to 800 °C (see Ref. [12]).

High-resolution XRD scans around the 006 and 012 peaks of PdCoO$_2$, shown in Figs. 3(c) and 3(d), respectively, reveal two additional effects that occur during the annealing process. The first is the overall change of the in-plane and out-of-plane lattice parameters. In going from the as-grown film to the 700 and 800 °C, the 006 peak shifted toward smaller 2θ, indicating a shift toward a larger out-of-plane lattice parameter (17.724 → 17.753 Å at 700 °C). As shown in Fig. 3(d), the in-plane lattice parameter showed the opposite trend, shifting toward larger 2θ and smaller lattice parameters (2.873 → 2.834 Å at 700 °C). The annealed values are closer to bulk PdCoO$_2$, indicating that either the films grow partially strained and annealing relaxes some of the residual strain, or defects, accumulated during the low-temperature growth, are accommodated by lattice distortion and relieved through annealing. Strain due to the Al$_2$O$_3$ substrate with an effectively smaller in-plane lattice parameter of 2.763 Å (i.e., $4.785/\sqrt{3}$) would tend to contract the PdCoO$_2$ to an in-plane lattice parameter that is smaller than bulk (2.830 Å),
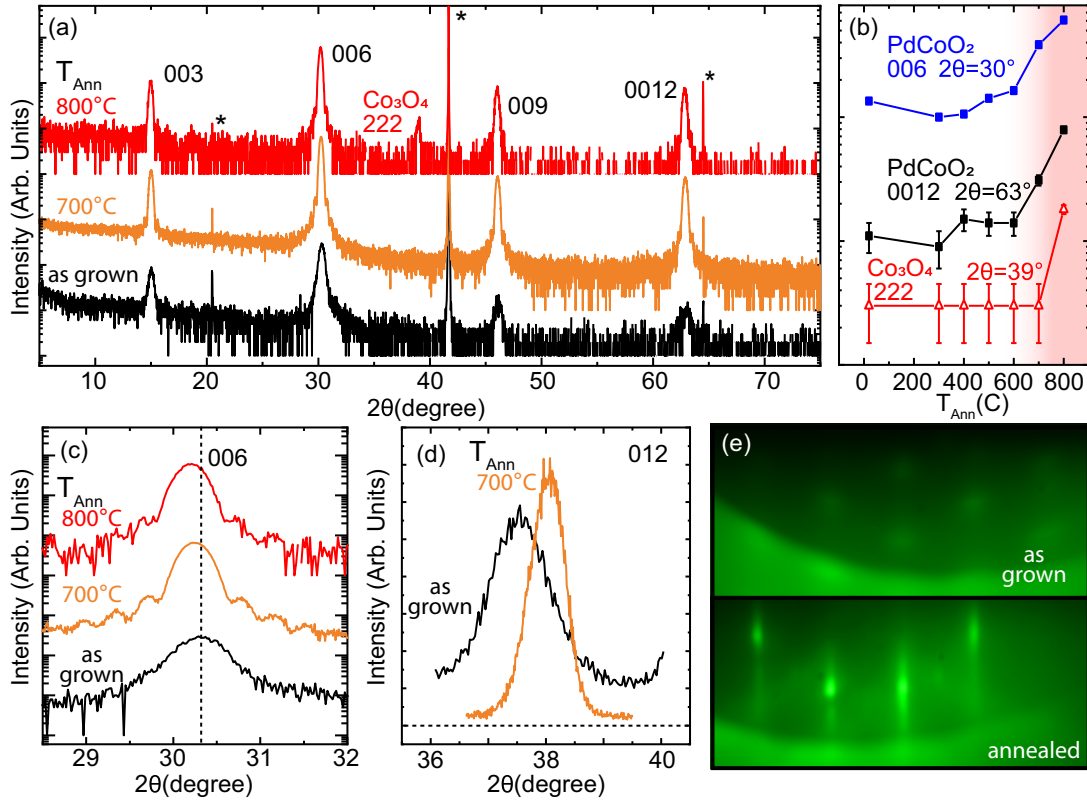
FIG. 3. Effect of air/oxygen annealing on crystallographic properties for $PdCoO_2$ films. (a) X-ray diffraction 2θ-θ scans for 25-nm-thick $PdCoO_2$ as grown at 300 °C (lower black curve labeled as-grown), annealed in air to a temperature of T_{ann} = 700 and 800 °C (orange and red curves, respectively). The $003n$ labels mark the delafossite peaks, and the asterisk (*) marks peaks belonging to Al_2O_3. Curves are vertically offset for clarity. (b) Intensity extracted from the curves in (a) plotted vs annealing temperature T_{ann} for the 006 and 0012 delafossite and 222 Co_3O_4 peaks. (c), (d) High-resolution x-ray diffraction about the 006 (c) and 012 (d) delafossite peaks. (e) Sample RHEED images taken along the $PdCoO_2$ $\langle 110 \rangle$ azimuthal direction for a 36-nm-thick film for as-grown (upper panel) vs oxygen-annealed (lower panel) (see Ref. [12]).

which would thus cause an expansion of the out-of-plane lattice parameter to a value larger than bulk (17.837 Å). Since this is inconsistent with the experimental observation for the as-grown films, the observed shift in lattice parameter is likely due to the elimination of defects through annealing. Further, this also confirms that the films are fully relaxed with respect to the Al_2O_3 structure.

The second observation that can be made from the data shown in Fig. 3(c) is the absence of Laue oscillations in the as-grown films, their appearance at 700 °C, and finally their partial suppression at 800 °C. The origin of Laue oscillations is coherent scattering from the surface of a film and the interface between the film and substrate, which requires atomically smooth surfaces. As discussed previously, and shown in Fig. 1(i), the surfaces of the films grown at 300 °C become rough and 3D-like for thick films. This is consistent with the absence of Laue oscillations in the as-grown films. Annealing mobilizes the surface atoms, likely favoring the formation of the low-energy 001 plane of $PdCoO_2$. This can be seen further in RHEED measurements performed on *ex situ* annealed films, shown in Fig. 3(e) (the film was taken out of the MBE chamber, annealed, then put back into the MBE system for subsequent RHEED measurements). The comparison of the as-grown film (top of the panel) with the postannealed film (bottom) shows that the surface flattened

and the crystal quality increased (indicated by much sharper diffraction peaks and the appearance of Kikuchi lines); it is noted that the postannealed films exhibit a weak second-order reconstruction. For the film annealed to 800 °C, the Laue oscillations were suppressed and became barely visible. This indicates surface roughening, which correlates with the XRD data shown in Fig. 3(a), where Co_3O_4 appeared at 800 °C. The two factors are likely connected and provide interesting insight into the synthesis of $PdCoO_2$. The Co_3O_4 formation was likely due to out-diffusion of palladium oxide, which may be predominately confined to the surface, and as such gives rise to roughening of the surfaces as Co_3O_4 nucleation likely starts there. In comparison to the synthesis of bulk $PdCoO_2$, which utilizes air annealing up to 950 °C [1,2,25], the observed formation of Co_3O_4 at 800 °C in thin films further suggests that it is confined to the surface region (this conjecture is also supported by transport measurements, discussed next). More precisely, if this was dictated by equilibrium thermodynamics, bulk crystals would exhibit similar impurities, and it is possible that bulk $PdCoO_2$ crystals have intrinsically Co-rich surfaces.

The residual resistivity for temperature near absolute zero is a very sensitive probe of crystal quality for metals as it only depends on the density of static disorder (crystal defects). Figure 4(a) shows temperature-dependent resistivity for the
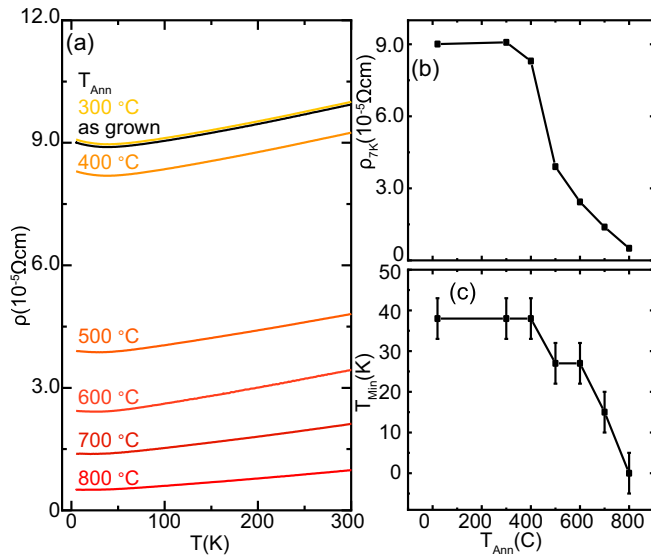
FIG. 4. Effect of air annealing on the transport properties of a PdCoO$_2$ film. (a) Resistivity vs temperature data for a 25-nm-thick PdCoO$_2$ film as-grown and annealed in air to a temperature of $T_{ann} = 300$–800 °C. (b) Resistivity as a function of T_{ann} taken at temperature 7 K. (c) The temperature at which the minimum of resistance occurs [extracted from the data in (a)] plotted as a function of T_{ann}.

same 25-nm-thick PdCoO$_2$ used for the XRD measurements in Fig. 3. The overall trend is a decrease in resistivity with decreasing temperature, reaching a finite resistivity as the temperature goes toward zero, which is typical of a metal. The overall trend with annealing is that the resistivity drops with increasing annealing temperature. The room-temperature resistivity decreases with increasing annealing temperature, going from around 98.0 $\mu\Omega$ cm for the as-grown films down to about 20.0 $\mu\Omega$ cm for the films annealed to 700 °C in air. For films annealed in oxygen at 800 °C, the room-temperature resistivity drops further to 4.7 $\mu\Omega$ cm (see Ref. [12]), which is comparable to the bulk crystal values, 2–8 $\mu\Omega$ cm [6,7,25–28]. With annealing, the low temperature value changed from 90.0 $\mu\Omega$ cm for the as-grown film down to 13.0 $\mu\Omega$ cm with 700 °C air annealing and to 1.1 $\mu\Omega$ cm with 800 °C oxygen annealing.

To expound on the evolution with increasing annealing temperature in air, the residual resistivity taken at $T = 7$ K, $\rho_{7\,K}$, is plotted versus annealing temperature T_{ann} in Fig. 4(b). With increasing annealing temperature, $\rho_{7\,K}$ does not change in going from as-grown to 300 °C, but beyond this it drops monotonically until 800 °C. Further, for the as-grown films it can be seen that $\rho_{7\,K}$ does not coincide with the minimum resistivity, as the minimum occurs at finite temperature T_{min}, below which there was a very shallow increase in the resistivity with decreasing temperature: the values of T_{min} are plotted versus T_{ann} in Fig. 4(c). The resistive minimum originates from, most likely, disorder-induced localization effects. This is consistent with the behavior of T_{min} shown in Fig. 4(b), where T_{min} is constant at about 40 K to 300–400 °C, and decreases monotonically toward zero up to 800 °C. Overall the dependences of $\rho_{7\,K}$ and T_{min} on T_{ann} are parallel to each other, but they differ with respect to the structural evolution shown in Fig. 3(b); more precisely, the structure is nominally

constant up to about 600 °C, above which the diffraction peaks increase as the crystal structure improves. The lower onset for the drop in $\rho_{7\,K}$ and T_{min} with increasing T_{ann} suggests that defects begin to reduce right above the growth temperature (300 °C). The difference between transport and XRD with annealing stems from the fact that transport and XRD are not sensitive to defects in the same way. For example, transport shows that defects began to be eliminated above 300 °C, but this is only evident in XRD for temperatures above 600 °C, pointing to either multiple types of defects with separate temperature dependency or to the fact that transport is more sensitive to defects; this interesting point requires a future systematic study of defect structures in PdCoO$_2$ thin films. Lastly, returning to the issue of Co$_3$O$_4$ segregation in the 800 °C sample, the improvement in resistivity in going from 700 to 800 °C shows that the Co$_3$O$_4$ segregation is not the limiting defect for the transport properties of these films, suggesting that they form highly localized islands, possibly confined to the surface: note also that with oxygen annealing, the film remains in single phase up to 800 °C (see Ref. [12]).

To understand the growth mode and defect structures in annealed films, thickness-dependent transport measurements are shown in Figs. 5(a) and 5(b), where $\rho_{7\,K}$ and RRR are plotted versus thickness, respectively. These data show that between 5 and 75 nm there is a strong thickness dependence, implying that the dominant scattering mechanism is from the surface. Above a thickness of about 100 nm, the resistivity saturated to a value of about 0.25 $\mu\Omega$ cm, which is the lowest among any metallic oxide thin films but still well above the best values attainable in bulk PdCoO$_2$ crystals (0.0075 $\mu\Omega$ cm) [7]. This is further reflected by the RRR value, which saturated to a maximum value of 16 (see, for example, Fig. S5), whereas bulk crystals can reach as high as ∼400 [7,27].

Saturation of the resistivity in the thick limit indicates that bulk defects, instead of surface scattering, are the limiting factor of the transport at low temperature in thick films. The most likely origin is epitaxial twins. These can be seen in the azimuthal (ϕ) scan about the {012} family of XRD peaks, which is shown in Fig. 5(c) for the PdCoO$_2$ film annealed to 700 °C. The Al$_2$O$_3$ substrate shows only three peaks, reflecting the threefold symmetry. In contrast, the PdCoO$_2$ film shows six peaks, indicating that there are two structural twins, labeled T_1 and T_2. The 012 T_1 and 012 T_2 peaks of PdCoO$_2$ appear at $\phi = \pm30°$ relative to the 012 peak of the Al$_2$O$_3$ structure. These twin domains can be seen explicitly in high-angle annular dark-field scanning transmission electron microscopy (HAADF STEM) images taken on an annealed film along the $\langle 100 \rangle$ crystal direction, shown in Figs. 5(d) and 5(e) (see Refs. [12] and [29] for details). In the wide scan, shown in Fig. 5(d), the Al$_2$O$_3$ substrate is the darker region and the PdCoO$_2$ film is the lighter upper portion. Here, the brightest atoms are the heavier Pd, and the lighter Co are the more diffuse atoms. In this image, the high crystalline quality of these films is apparent, as the layered PdCoO$_2$ structure is clearly visible. Moreover, domain boundaries are clearly visible both vertically and horizontally relative to the PdCoO$_2$ layers. In the zoomed-in image in Fig. 5(e) [taken from the box in Fig. 5(d)] these boundaries are highlighted by yellow arrows. These domains are clearly identified as T_1 and T_2 by overlaying the crystal structure of PdCoO$_2$ projected along the
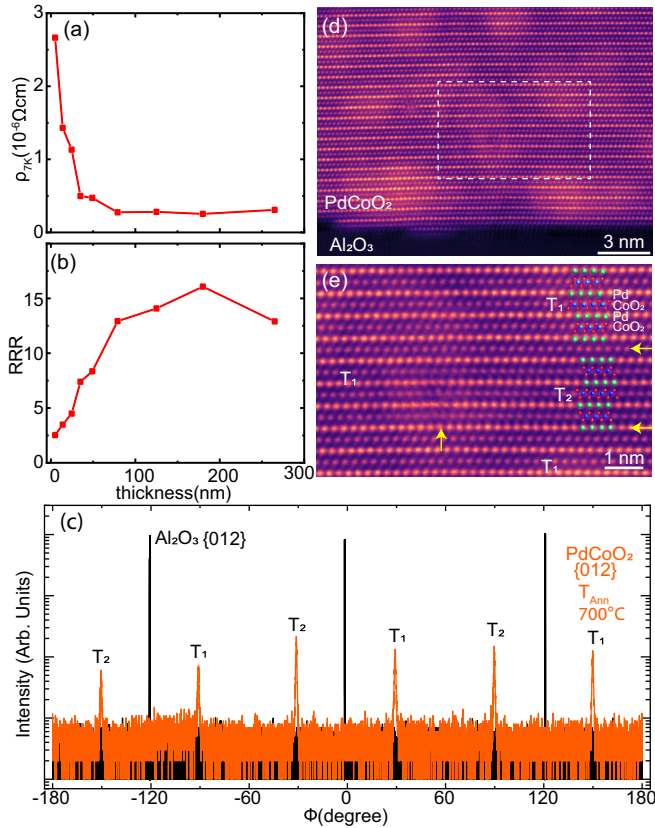
FIG. 5. Transport and structural properties of air/oxygen annealed $PdCoO_2$ films. (a), (b) Resistivity vs film thickness plots of $PdCoO_2$ films annealed in oxygen at $800\,°C$, taken at a temperature of 7 K (a) and the residual resistivity ratio (RRR) (b). (c) X-ray diffraction azimuthal scan (ϕ) taken about the {012} peaks for a $PdCoO_2$ film annealed to $700\,°C$ (orange curve) and the {012} peaks Al_2O_3 substrate (black curve). The $PdCoO_2$ twin domains are distinguished by the labels T_1 and T_2. (d), (e) HAADF STEM taken along the $\langle 100 \rangle$ zone axis. (d) Wide scale image showing the $PdCoO_2$ film and the Al_2O_3 substrate. (e) Zoom-in of the boxed region in (d). In this image, the $PdCoO_2$ atomic positions are overlaid on the image where both T_1 and T_2 domains are shown, and domain boundaries are highlighted by the yellow arrows.

$\langle 100 \rangle$ direction, and the $\langle \bar{1}00 \rangle$ direction on top of the STEM data, where there is excellent agreement on the atom positions. The origin of the twins is due to equivalent ways for both T_1 and T_2 to epitaxially match Al_2O_3 (as shown in Fig. S6 in Ref. [12]), the formation of stacking faults (see, for example, Refs. [30,31]), or a combination of the two. Such twins are also observed in previous PLD grown films [10].

To conclude, we have shown that, although challenging, there is a route to growing $PdCoO_2$ epitaxial films by MBE on Al_2O_3. This required overcoming the primary challenge of oxidizing Pd. It was found that this limited the *in situ* growth temperature to about $300\,°C$, which was insufficient to drive diffusion, and thus necessitates an *ex situ* postgrowth anneal to high temperatures to create films with high crystalline quality. These films exhibit improved transport properties compared with the previous PLD grown films [10]. Specifically, the room-temperature resistivity of the annealed films approaches

that of the best single crystals, suggesting comparable crystalline quality, as confirmed by the STEM data. However, the transport properties at low temperature were likely limited by the formation of structural twins, which originates from the epitaxial relationship between the film and the substrate: there are two equivalent motifs to orient $PdCoO_2$ on Al_2O_3. In the context of future research directions, this work points out several key factors. (i) Growing the full class of metallic delafossites, including the Pt compounds and $AgNiO_2$, is likely more challenging than the Pd-based material shown here, since both Pt and Ag are more difficult to oxidize than Pd. But as the current work has shown, it may be possible with a low-temperature growth followed by a postanneal in high oxygen pressure. Moreover, since Pt-oxides and Ag-oxides are nonvolatile, unlike PdO, higher oxygen pressures and higher temperatures may enable the formation of high-quality films of these delafossites. (ii) Improving the crystal quality of $PdCoO_2$ may require moving away from Al_2O_3 as a substrate. Although a delafossite-based buffer may seem viable, such domains would always be present as they result from the structural mismatch between delafossite and Al_2O_3; thus, realizing single-domain $PdCoO_2$, and other metallic delafossites, likely necessitates the development of delafossite single-crystal substrates. (iii) Due to the rich surface physics in these materials [9,32], there are many open questions regarding the structural and electronic effects of surface termination and layering sequence. Altogether, the successful synthesis of high-quality metallic delafossite films as demonstrated here will enable a range of fundamental studies that cannot be accessed with bulk crystals in this rich family of layered, triangular oxides.

[1] R. D. Shannon, C. T. Prewitt, and D. B. Rogers, Inorg. Chem. **10**, 719 (1971).

[2] R. D. Shannon, D. B. Rogers, C. T. Prewitt, and J. L. Gillson, Inorg. Chem. **10**, 723 (1971).

[3] A. Stadler, Materials (Basel) **5**, 661 (2012).

[4] H. Kawazoe, M. Yasukawa, H. Hyodo, M. Kurita, H. Yanagi, and H. Hosono, Nature (London) **389**, 939 (1997).

[5] Y. J. Shin, J. P. Doumerc, P. Dordor, C. Delmas, M. Pouchard, and P. Hagenmuller, J. Solid State Chem. **107**, 303 (1993).

[6] A. P. Mackenzie, Rep. Prog. Phys. **80**, 032501 (2017).

[7] C. W. Hicks, A. S. Gibbs, A. P. Mackenzie, H. Takatsu, Y. Maeno, and E. A. Yelland, Phys. Rev. Lett. **109**, 116401 (2012).

[8] L. Balents, Nature (London) **464**, 199 (2010).

[9] V. Sunko, H. Rosner, P. Kushwaha, S. Khim, F. Mazzola, L. Bawden, O. J. Clark, J. M. Riley, D. Kasinathan, M. W. Haverkort, T. K. Kim, M. Hoesch, J. Fujii, I. Vobornik, A. P. Mackenzie, and P. D. C. King, Nature (London) **549**, 492 (2017).

[10] T. Harada, K. Fujiwara, and A. Tsukazaki, APL Mater. **6**, 046107 (2018).

[11] L. Zhang, Y. Zhou, L. Guo, W. Zhao, A. Barnes, H.-T. Zhang, C. Eaton, Y. Zheng, M. Brahlek, H. F. Haneef, N. J. Podraza, M. H. W. Chan, V. Gopalan, K. M. Rabe, and R. Engel-Herbert, Nat. Mater. **15**, 204 (2016).

[12] See Supplemental Material at http://link.aps.org/supplemental/10.1103/PhysRevMaterials.3.093401 for experimental details and supplemental data.

[13] C. R. Abernathy, S. J. Pearton, F. Ren, W. S. Hobson, T. R. Fullowan, A. Katz, A. S. Jordan, and J. Kovalchick, J. Cryst. Growth **105**, 375 (1990).

[14] C. D. Theis, J. Yeh, D. G. Schlom, M. E. Hawley, and G. W. Brown, Thin Solid Films **325**, 107 (1998).

[15] E. H. Smith, J. F. Ihlefeld, C. A. Heikes, H. Paik, Y. Nie, C. Adamo, T. Heeg, Z.-K. Liu, and D. G. Schlom, Phys. Rev. Mater. **1**, 023403 (2017).

[16] H. P. Nair, Y. Liu, J. P. Ruf, N. J. Schreiber, S.-L. Shang, D. J. Baek, B. H. Goodge, L. F. Kourkoutis, Z.-K. Liu, K. M. Shen, and D. G. Schlom, APL Mater. **6**, 046101 (2018).

[17] D. G. Schlom, APL Mater. **3**, 062403 (2015).

[18] M. Brahlek, A. Sen Gupta, J. Lapano, J. Roth, H.-T. Zhang, L. Zhang, R. Haislmaier, and R. Engel-Herbert, Adv. Funct. Mater. **28**, 1702772 (2018).

[19] C. P. Flynn, J. Phys. F **18**, L195 (1988).

[20] C. A. F. Vaz, V. E. Henrich, C. H. Ahn, and E. I. Altman, J. Cryst. Growth **311**, 2648 (2009).

[21] H.-J. Noh, J. Jeong, J. Jeong, E.-J. Cho, S. B. Kim, K. Kim, B. I. Min, and H.-D. Kim, Phys. Rev. Lett. **102**, 256404 (2009).

[22] R. W. Grimes and K. P. D. Lagerlof, J. Am. Ceram. Soc. **74**, 270 (1991).

[23] M. J. Redman and E. G. Steward, Nature (London) **193**, 867 (1962).

[24] W. L. Smith and A. D. Hobson, Acta Crystallogr. Sect. B **29**, 362 (1973).

[25] R. D. Shannon, D. B. Rogers, and C. T. Prewitt, Inorg. Chem. **10**, 713 (1971).

[26] M. Tanaka, M. Hasegawa, and H. Takei, Czech. J. Phys. **46**, 2109 (1996).

[27] H. Takatsu, S. Yonezawa, S. Mouri, S. Nakatsuji, K. Tanaka, and Y. Maeno, J. Phys. Soc. Jpn. **76**, 104701 (2007).

[28] H. Takatsu, J. J. Ishikawa, S. Yonezawa, H. Yoshino, T. Shishidou, T. Oguchi, K. Murata, and Y. Maeno, Phys. Rev. Lett. **111**, 056601 (2013).

[29] C. Ophus, J. Ciston, and C. T. Nelson, Ultramicroscopy **162**, 1 (2016).

[30] R. Ramlau, R. Schneider, J. H. Roudebush, and R. J. Cava, Microsc. Microanal. **20**, 950 (2014).

[31] J. H. Roudebush, N. H. Andersen, R. Ramlau, V. O. Garlea, R. Toft-Petersen, P. Norby, R. Schneider, J. N. Hay, and R. J. Cava, Inorg. Chem. **52**, 6083 (2013).

[32] F. Mazzola, V. Sunko, S. Khim, H. Rosner, P. Kushwaha, O. J. Clark, L. Bawden, I. Marković, T. K. Kim, M. Hoesch, A. P. Mackenzie, and P. D. C. King, Proc. Natl. Acad. Sci. USA **115**, 12956 (2018).

[33] http://energy.gov/downloads/doe-public-access-plan.